JMEPEG (2006) 15:632-639
DOI: 10.1361/105994906X150876

1059-9495/$19.00

Modification of a Thermomechanical Model to Predict Constitutive Behavior of Al-Mg-Si Alloys

J. van de Langkruis, W.H. Kool, and S. van der Zwaag

(Submitted March 14, 2006; in revised form April 11, 2006)

A previously developed constitutive model for quantification of the effect of the condition of Mg and Si in AA6*xxx* alloys was used for the prediction of the flow stresses measured by plane strain compression (PSC) tests. As an extension of earlier work, two AA6*xxx* alloys were subjected to different thermal pretreatments and were plane strain compression tested at temperatures and strain rates typical for hot extrusion. Heating rates to the test temperature were varied. Dissolution behavior of the β precipitates, needed for the quantification, was experimentally validated using differential scanning calorimetry. Significant differences in flow stress during PSC testing were observed as a function of the heating rate to the deformation temperature and of the different conditions that resulted from the different thermal pretreatments. The model was also applied to the combined set of present data and data reported earlier. This combined set of data encompasses a wide range of alloy compositions and thermal histories. It is found that the model gives a fair prediction. Excellent agreement was obtained by assuming that the parameter describing the solution hardening behavior in the model is temperature dependent instead of constant.

Keywords AA6*xxx*, constitutive model, plane strain compression, solution hardening

1. Introduction

Billet homogenization precedes industrial extrusion (or rolling) of DC-cast aluminum billets. During homogenization of AA6*xxx* alloys, phase transformation of the Al(Fe,Mn)Si-intermetallics takes place and the Mg and Si solute contents increase by dissolution of β Mg-Si particles (Ref 1, 2). During subsequent cooling to room temperature after homogenization, β′ and β Mg-Si particles may precipitate (Ref 3-5), which reduces the Mg and Si solute content. Additional precipitation or dissolution may take place during heating up and preheating of the billet prior to extrusion (Ref 6-10).

Extrusion pressure and mechanical properties of the extrudate depend on the condition of Mg and Si before extrusion, defined as the presence of Mg and Si either as solute or bound as precipitates.

In previous work (Ref 11, 12), the effect of the condition of Mg and Si in an AA6063 alloy was investigated for isothermal laboratory-scale extrusion and with plane strain compression (PSC) tests. It was shown that differences in solute content resulted in differences in the extrusion pressure and in the flow stress, measured by PSC tests just before extrusion. Differences in extrusion pressure and flow stress were proportional, indicating a direct connection between flow stress measured before extrusion and extrusion pressure.

In other studies, flow stresses were determined by PSC testing at elevated temperatures on specimens with different conditions of Mg and Si (Ref 6, 13). One paper (Ref 13) concentrated on various constitutive equations and assessed their capability for modeling purposes. It was concluded that use of a hyperbolic-sine law (Ref 14) was the most favorable. To account for the effect of the condition of Mg and Si, a modification of the hyperbolic-sine law was proposed (Ref 13) by introduction of a "weighted solute content" that accounts for the effect of Mg and Si solution hardening. In this way, flow stress was modeled for different Al-Mg-Si alloys and for conditions where solute levels were in equilibrium at the testing temperature just before the test. In another paper (Ref 6), an AA6063 alloy was subjected to different heat treatments to induce various types of precipitates. A validated particle dissolution model developed by Vermolen et al. (Ref 7-9) was used to determine the solute content just before the PSC test, considering that for these experiments solute levels changed during heating up of the specimens to the test temperature. Good agreement was found between measured flow stress and flow stress calculated with the modified hyperbolic-sine law, using the parameter set found earlier (Ref 13).

The objective in this study is to extend the previous work to a wider range of preheating conditions and AA6*xxx* alloys. Flow stresses are determined from PSC tests. Hardness is also measured. Modeling of the flow stress data using the adapted hyperbolic-sine law was done for the present data in combination with the data determined earlier (Ref 6, 13). Solute levels were modeled using the particle dissolution model developed by Vermolen et al. (Ref 7-9). Two critical parameters in this model were derived from differential scanning calorimetry (DSC) experiments. It is noted that in relation to the present PSC measurements, industrial-scale extrusion experiments have also been performed, and these are described elsewhere (Ref 15).

2. Experimental Procedures

2.1 Materials and Material Preparation

In the present experiments, two alloys—AA6005 and AA6063—were used with compositions as given in Table 1.

J. van de Langkruis, Corus Research, Development and Technology, IJmuiden, The Netherlands; **W.H. Kool,** Department of Materials Science and Engineering, Delft University of Technology, Rotterdamseweg 137, NL-2628 AL, Delft, The Netherlands; and **S. van der Zwaag,** Delft University of Technology, Faculty of Aerospace Engineering, Delft, The Netherlands. Contact e-mail: jorgen.van-delangkruis@corusgroup.com.

Table 1 Composition of AA6005 and AA6063 alloys (wt.%)

Alloy	Mg	Si	Fe	Mn	Other
AA6005	0.69	0.88	0.29	0.18	<0.08
AA6063	0.48	0.36	0.23	0.06	<0.11

The alloys were hot-top cast into round billets with a diameter of 20 cm.

For the PSC experiments, rectangular specimens, 130 × 70 × 12 mm, were machined from the billets. The specimens were homogenized at 853 ± 5 K for 6 h and water quenched. A part of the specimens was subsequently pre-aged for 24 h at either 598 K [condition β(1)] or 723 K [condition β(2)] to induce a more refined (598 K) or a coarser (723 K) distribution of β-Mg_2Si particles. Pre-aging was followed by a water quench. For the nontreated specimens (condition WQ), it is assumed that Mg and Si were in solid solution.

For the DSC experiments, disc-shaped specimens, diameter 6 mm and thickness 0.6 mm, were taken from the billets. Similar heat treatments as for the PSC specimens were applied in situ in the DSC apparatus.

From the deformed region of the PSC specimens, samples were taken and artificially aged at 458 K for 6 h (T5). After ageing, Vickers hardness was measured (load 10 N).

2.2 DSC Experiments

DSC experiments were performed for determining the equivalent spherical particle size r_0 and the cell size R_{Al}, which are parameters needed in the particle dissolution model (Ref 7-9). For the experiments, all heat treatments took place in situ, according to procedures described elsewhere (Ref 16). Similar treatments as applied to the PSC samples were performed to produce similar microstructures. The quenching rate was ~200 K/min (Ref 16). These treatments were immediately followed by a scan from 273 to 853 K with a heating rate of 20 K/min. For a particular alloy, only one single specimen was used. After a DSC scan, the specimen was first solutionized before a new pre-aging treatment was applied. The values of r_0 and R_{Al} were determined by matching the experimental dissolution peaks to the calculated dissolution contours according to the procedure described earlier (Ref 10).

2.3 PSC Experiments

PSC tests were performed in duplicate using the thermomechanical treatment simulator (TMTS) apparatus at Corus, IJmuiden (Ref 17). Test temperatures were 673 or 793 K, the equivalent tensile strain rate was 100 s^{-1}, and tests were done to a maximum equivalent tensile strain of 1.2. At the contact surface between the tools and the specimen, a graphite/water-based lubricant was applied.

Before deformation, the specimens were heated with a heating rate of 4.5, 18, or 180 K/min to the testing temperature by induction heating in a separate furnace. When the testing temperature was reached, the specimens were immediately placed into the compression unit, which was set at the testing temperature, and deformed within 1 s. After deformation, the specimens were water quenched to room temperature. From these specimens, samples were taken from the deformed area and peak aged at 458 K (6 h). The temperature during preheating and testing was measured with two K-type thermocouples placed in holes located in the center and 20 mm away from the center of the specimens, drilled at the specimen side. During deformation, the temperature, applied load, and tool displacement in the axial direction were registered. Tool displacement was controlled in such a way that a constant (true) strain rate was obtained. The load-displacement data in the PSC test were transformed into stress-strain curves after the procedure described elsewhere (Ref 17). The procedure corrects for lateral spread and friction at the specimen-tool interface. A friction coefficient of $\mu = 0.3$ was assumed. From each stress-strain curve, a characteristic flow stress at a fixed strain value of $\varepsilon = 1$ was taken. The reproducibility of this characteristic flow stress was typically 2 MPa.

Deformation heating was expected to occur during compression (Ref 18). However, because the strain rate was 100 s^{-1}, the temperature increase due to deformation heating could not be monitored fast enough. For all data points in the stress-strain curves, deformation heating was calculated assuming a 55% conversion into heat of the work performed (Ref 6). Flow stress values were corrected for these temperature deviations using an exponential law (Ref 13, 19). It was found that, at a strain of 1, this correction was typically about 3 MPa at 793 K and 8 MPa at 673 K. For the various conditions, also Vickers hardness (HV 1 kg) was measured.

2.4 Modeling

The PSC flow stress values were modeled as a function of the strain rate $\dot{\varepsilon}$, temperature T, and the solute content during deformation, using a modified hyperbolic sine law (Ref 14). This law was adapted for the effect of solution hardening by Mg and Si atoms (Ref 6, 13) and reads:

$$\sigma_f = \frac{1}{\gamma}\ln\left\{\left(\frac{Z}{A}\right)^{1/m} + \left[\left(\frac{Z}{A}\right)^{2/m} + 1\right]^{1/2}\right\}$$

$$Z = \dot{\varepsilon}\exp\left(\frac{Q}{RT}\right) \qquad \text{(Eq 1)}$$

$$A = \exp(K_1)\exp(-K_2X)$$

$$X = 2[\text{Mg}] + [\text{Si}]$$

where σ_f is flow stress, g and m are strain rate sensitivity parameters, assumed constant in the experimental regimen, Z is the Zener-Hollomon parameter, $\dot{\varepsilon}$ is the strain rate, Q is the apparent activation energy of the deformation process during plastic flow, R is the universal gas constant, T is the absolute temperature, and A is a prefactor depending explicitly on the Mg and Si matrix solute content. The quantity X is the weighted solute content in the aluminum matrix, K_1 and K_2 (wt.%$^{-1}$) are constant model parameters, and [Mg] and [Si] are the solute contents of Mg and Si in the matrix, both in wt.%. Values were taken identical to those in previous work (Ref 6) and are summarized in Table 2.

The solute Mg and Si content in the matrix during hot deformation was calculated as a function of the initial condition of Mg and Si and the temperature-time path before deformation, using the particle dissolution model of Vermolen et al. (Ref 7-10). In the calculation, the alloy was simplified to a system consisting of a spherical Mg_2Si precipitate centered in

a spherical aluminum matrix cell. The solute Mg and Si content of the matrix and the volume fraction of the particle in the cell were calculated using the thermodynamic program MTDATA (Ref 11, 13, 20). It was verified that the influence of Si precipitates on the solute contents and Mg_2Si volume fractions could be neglected. The values of the radii of the particle (r_0) and cell (R_{Al}) in the particle dissolution model were estimated from the DSC curves.

2.5 Modification of the Model

In section 4.1, the present dataset plus three datasets from other publications (Ref 6, 11, 13) are combined and reexamined, using the model given in Eq 1. These datasets are also reexamined with the assumption that the effect on flow stress of the weighted solute content is temperature dependent, i.e., a temperature-dependent K_2 is introduced according to:

$$K_2 = a/T + b \quad \text{(Eq 2)}$$

where constants a (K wt.%$^{-1}$) and b (wt.%$^{-1}$) are fitting parameters.

Table 2 Parameter values used in the constitutive modeling

Parameter	Value	Dimension
m	4.49	…
γ	0.0324	MPa^{-1}
Q	158	kJ/mol
K_1	27.7	wt.%$^{-1}$
K_2	2.5	wt.%$^{-1}$

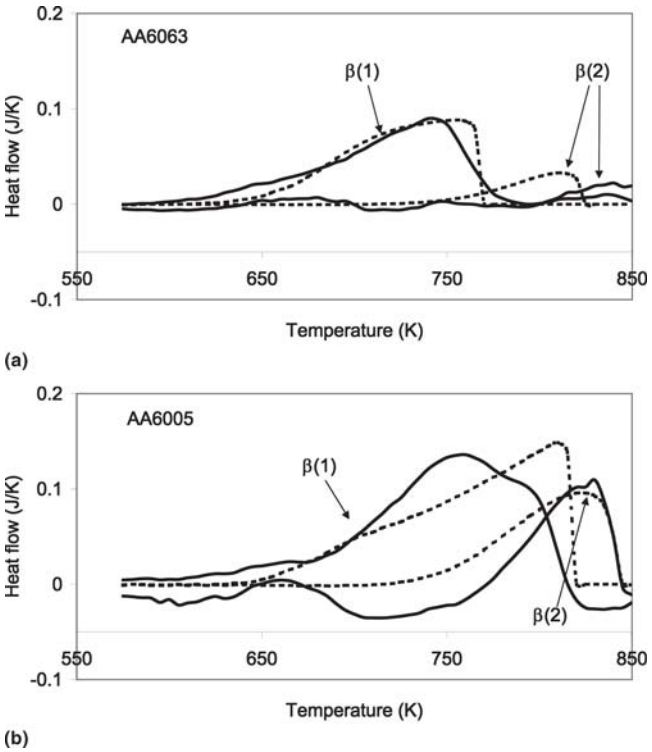

Fig. 1 DSC spectra of (a) AA6063 and (b) AA6005 for β(1) and β(2) conditions (solid line, experiment; dotted line, model)

3. Results

3.1 Evaluation of Initial Microstructure

In Fig. 1, the DSC spectra of the β(1) and β(2) specimens are shown for both alloys. The β(1) spectrum displays a β dissolution peak (Ref 16, 21-23) at 746 K (AA6063) or 763 K (AA6005). The difference in peak temperatures is due to the difference in solvus temperature, and the difference in peak area is due to the difference in Mg and Si content. The onset temperature of the β(1) peak (~600 K) is close to the corre-

Table 3 Values for r_0 and R_{Al} and volume fraction of β precipitates

Alloy	Pre-treatment condition	r_0, nm	R_{Al}, nm	Volume fraction precipitates
AA6063	β (1)	200	1048	0.0070
AA6063	β (2)	1000	6850	0.0031
AA6005	β (1)	200	914	0.0105
AA6005	β (2)	1000	4980	0.0081

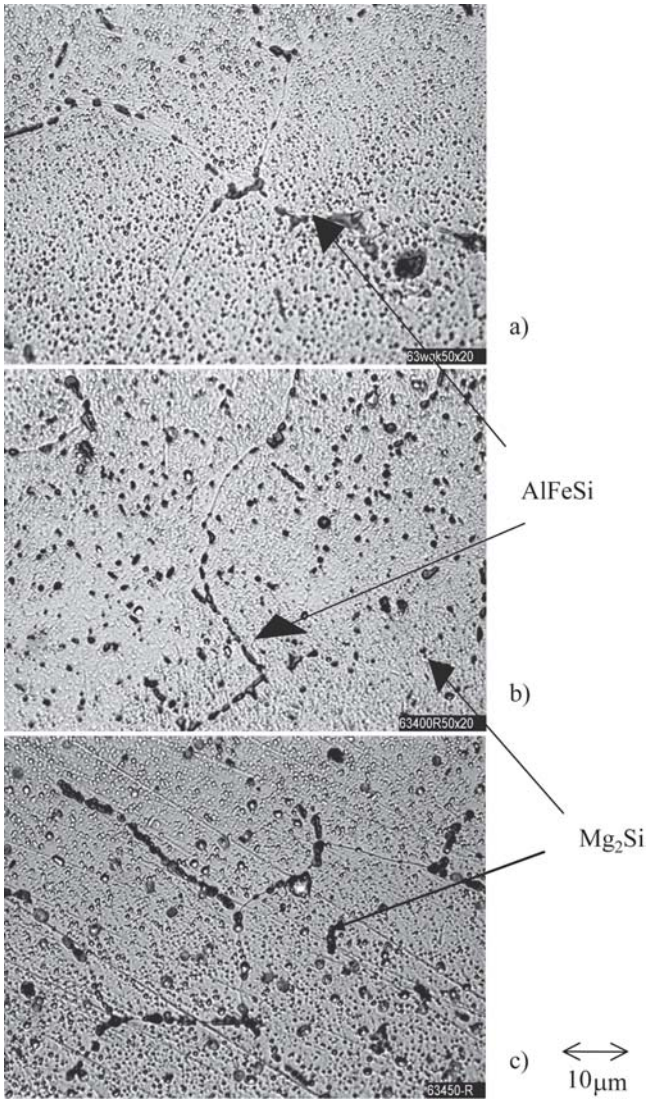

Fig. 2 Optical micrographs of the AA6005 alloy for the conditions (a) WQ, (b) β(1), and (c) β(2)

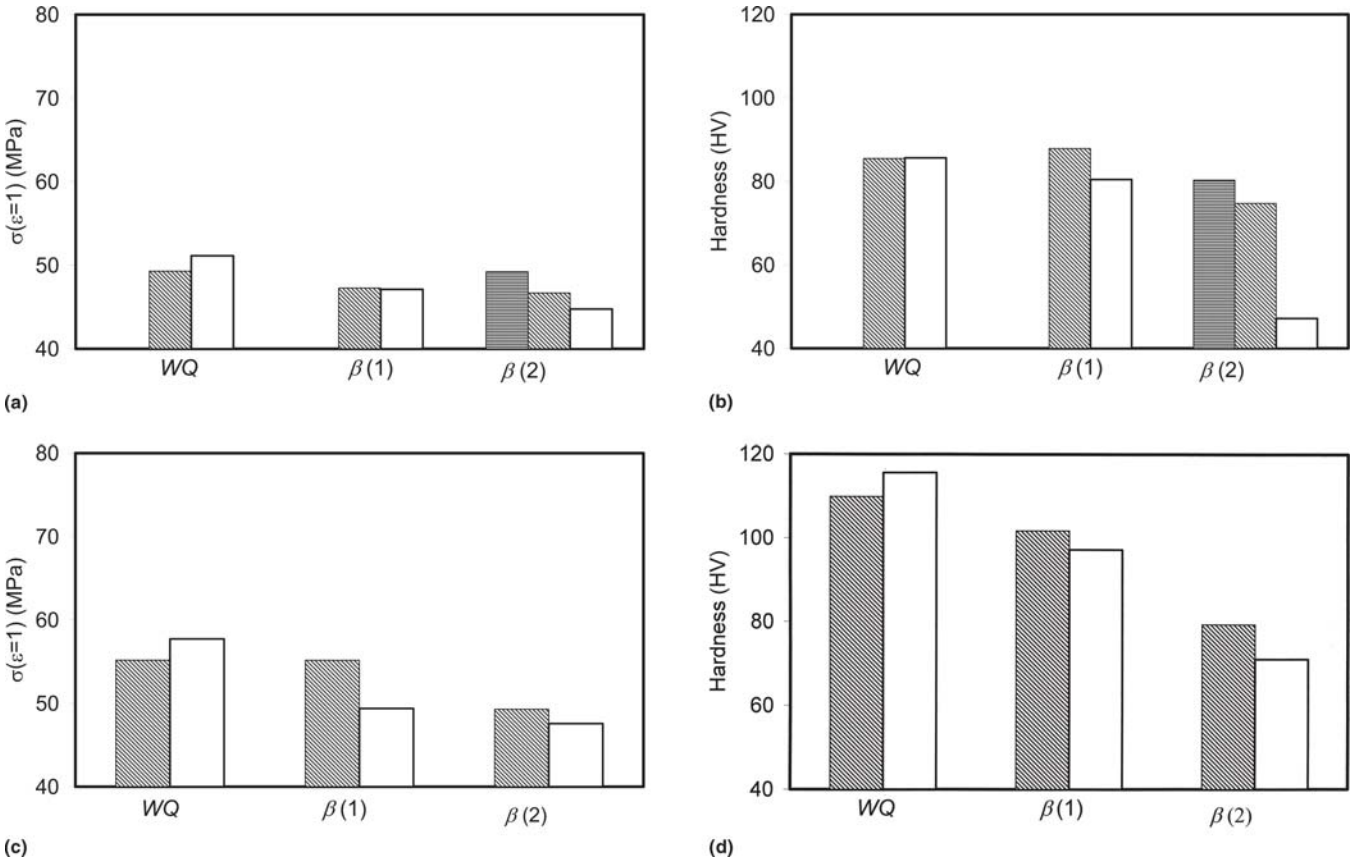

Fig. 3 Flow stress at $\varepsilon = 1$ during PSC testing at 793 K and Vickers hardness after subsequent aging as a function of the initial material condition: (a) AA6063, flow stress; (b) AA6063, Vickers hardness; (c) AA6005, flow stress; and (d) AA6005, Vickers hardness. Heating rates, 4.5 (▤), 18 (▧), and 180 K/min (□)

sponding pre-aging temperature, indicating that the equilibrium volume fraction of precipitates was reached during pre-aging. The β(2) curve of the AA6005 alloy shows a clear β dissolution peak at 828 K, whereas the β(2) curve of the AA6063 alloy shows only a minor β dissolution peak. This is attributed to the low amount of β precipitation as a consequence of the lower alloying content in AA6063 and the high pre-aging temperature (723 K) of the β(2) condition.

The values of the initial particle radius r_0 and the cell size R_{Al} were determined by matching these curves to the calculated dissolution contours, which are also given in Fig. 1. The best fit was obtained with the r_0 and R_{Al} values given in Table 3. It is found that r_0 and R_{Al} increase with increasing pre-aging temperature, both reflecting the coarser distribution of the particles at higher pre-aging temperature. The volume fraction of precipitates is smaller for AA6063 and for the β(2) condition.

In Fig. 2, optical micrographs are given of both conditions of the AA6005 alloy. Large intermetallics are present that contain Al, Fe, Mn, and Si. Between these particles, smaller β particles can be observed with finer [β(1)] or coarser [β(2)] distribution. For the WQ condition, β particles were absent. The largest β particles are 1-2 μm in size. The micrographs of the AA6063 alloy show similar trends but with lower particle densities.

It is concluded that the pretreatments have led to the intended Mg and Si distributions, i.e., condition β(1) with smaller and more numerous β precipitates and condition β(2) with larger and less numerous precipitates. As expected, alloy AA6005 contains a higher volume fraction of precipitates.

3.2 Flow Stress During Plane Strain Compression and Hardness

In Fig. 3, the flow stress values determined at 793 K and a strain ε equal to 1 are given for both alloys. Vickers hardness of the PSC deformed specimens is given as well after the peak aging. Figure 3(a) shows that, for the AA6063 alloy the flow stress becomes lower in the order WQ > β(1) > β(2), which reflects a decreasing solution hardening in the specimens. However, in section 3.1, it was seen that before heating to the PSC test temperature the solute level for the β(2) condition was higher than for the β(1) condition. A change in solute levels takes place during the heating up to the test temperature because, due to the finer distribution of the β(1) particles, these particles dissolve faster during heat up (Section 3.3). Flow stresses for both β(1) and β(2) conditions decrease with increasing heating rate because dissolution and consequently solution hardening are reduced. These solute effects are mirrored in the hardness after peak aging of the AA6063 alloy (Fig. 3b), because the precipitation hardening effect is determined by the solid solution level. It is assumed that, during the test, the amount of solid solution will hardly change due to the short time involved.

Figure 3(c) and (d) show for the AA6005 alloy the same trends as with the AA6063 alloy. Values are somewhat higher due to the higher alloying content. For the WQ condition of the AA6005 alloy, both flow stress and Vickers hardness tend to be slightly lower after heating with a low rate (18 K/min) than with a high rate (180 K/min). Apparently, some precipitation

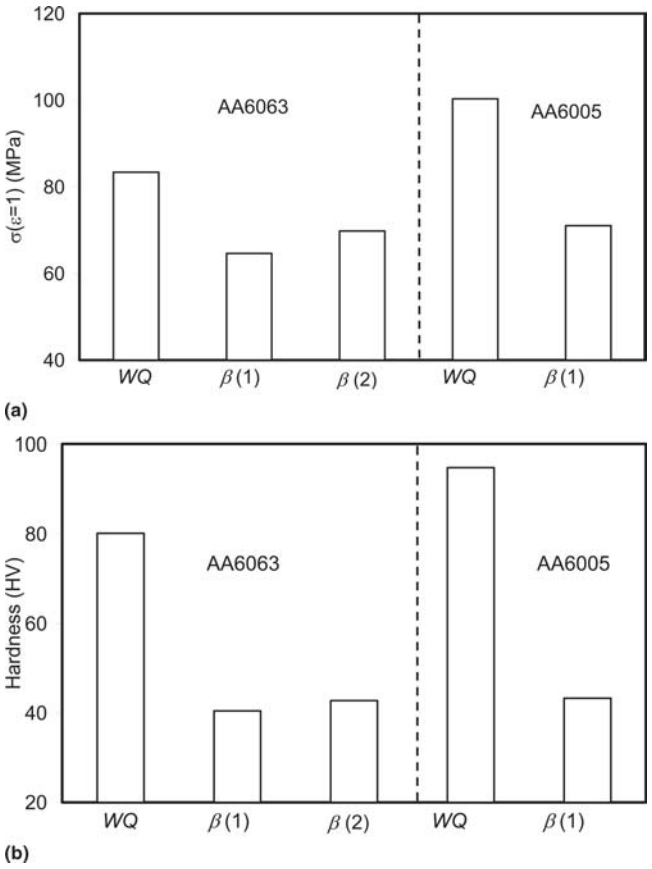

Fig. 4 Flow stress at $\varepsilon = 1$ during PSC testing at 673 K and Vickers hardness after subsequent ageing as a function of the initial material condition for AA6063 and AA6005: (a) flow stress, (b) Vickers hardness. Heating rate, 180 K/min

occurs during heating up with the low heating rate as, for this alloy, the solvus temperature is somewhat higher than the deformation temperature.

In Fig. 4, the flow stress values determined at 673 K and a strain ε equal to 1 are given for both alloys. Also, Vickers hardness of the PSC-deformed specimens is given after the peak aging. The heating rate was 180 K/min. Flow stresses decrease in the order WQ > β(2) > β(1). In contrast with the experiments at 793 K, the heating rate is so high and the testing temperature is so low that particle dissolution effects during heat up are negligible. Therefore, the solute contents during PSC testing will be equal to those of the initial conditions and will decrease in the order WQ > β(2) > β(1). The differences in flow stress and hardness between the two alloys at 673 K are pronounced for the WQ condition due to the difference in solute content. They are smaller for the pre-aged conditions due to more comparable solute content in both alloys (Section 3.3).

3.3 Modeling PSC Results

Figure 5 shows the change of the weighted solute contents X, calculated with the particle dissolution model of Vermolen et al. (Ref 7-9) during the heat-up phase before the PSC test. The initial level of the weighted solute content, which is the level after the pre-aging step, was calculated using MTDATA. A linear heating rate in the heat-up phase was applied. It is seen that initial solute levels are higher for the β(2) condition than for the β(1) condition due to the higher pre-aging temperature and they are higher for AA6005 than for AA6063 due to the higher alloying content. During the heat-up phase, dissolution is stronger for the lower heating rates (longer dissolution times). Dissolution is faster for β(1) than for β(2) due to the smaller initial particle size. Figure 5 demonstrates that, after heating up for the PSC test at 673 K, for most conditions (but not all) the solute content will be equal to the initial content, whereas for the PSC test at 793 K the content changes and often reaches the equilibrium content at 793 K. Comparing Fig. 5(a) with (b), it is seen that for a specific heating rate the initial solute level of the β(1) condition is lower than that of the β(2) condition, whereas this trend has reversed after heating up to the testing temperature of 793 K. This effect was noted in section 3.2 and also in earlier work (Ref 6) and explains the behavior in flow stress and peak hardness.

The solute contents, calculated with the particle dissolution model were incorporated into the constitutive model (Eq 1). They were assumed not to change during PSC testing because testing occurred in a short time (~0.012 s). Figure 6 shows the experimental flow stress values of both alloys at a fixed strain ε of 1, together with the values calculated with the constitutive model. Fair agreement existed between the experimental data and the model predictions. There is a strong dependence of the flow stress with the weighted solute content. The relationship between flow stress and weighted solute content appears to be independent of the alloy.

4. Discussion

4.1 Constitutive Modeling of PSC Results

Figure 7(a) combines both the present data and the data reported elsewhere (Ref 6, 11, 13) and shows the calculated flow stress against the experimentally determined flow stress. Calculation was done using Eq 1 and the parameters given in section 2.4. For some previously reported data (Ref 11, 13), parameter K_1 was slightly adjusted to reflect differences in sample geometry and friction coefficient. The complete data set encompasses several alloys, such as AA6063, AA6005, AlMg0.44Si0.22, AlMg0.77Si0.39, AlMg1.05Si0.29, and AlSi1.35Mg0.40, and also different conditions, such as homogenized and quenched, aged at various temperatures, over-aged/annealed, and changed during heating to the test temperature. Good agreement is obtained, but the trend of the data points deviates slightly from the ideal line, leading to some overestimation of the flow stress at low flow stresses and some underestimation at high flow stresses.

On the basis of this observation, it is thought that the effect of the weighted solute content on the flow stress such as given in Eq 1 is temperature dependent, i.e., that K_2 should be temperature dependent. In Section 2.5, a simple modification was proposed, introducing instead of a constant fitting parameter, K_2, two fitting parameters, a and b, according to Eq 2. In Fig. 7(b), the result is shown for $a = 5255$ K and $b = -5.5$. The figure shows that, for the complete dataset, the predictive capability for estimating the hot flow stress is excellent.

4.2 Solution Effects During Hot Deformation

In the modeling, it is assumed that the condition of solute just before the hot deformation determines the load needed

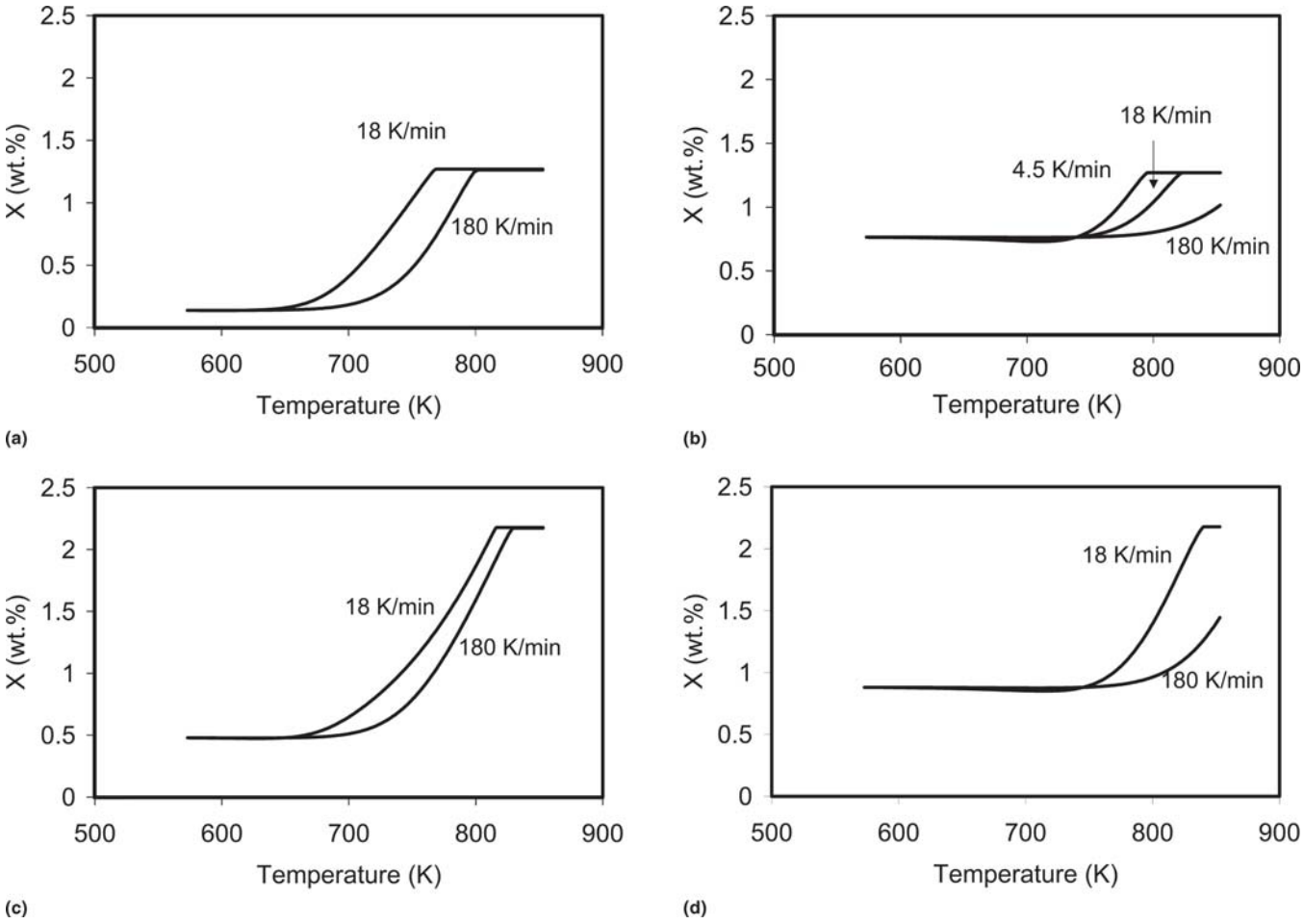

Fig. 5 Solute content during linear preheating for the heating rates applied: (a) β(1), AA6063; (b) β(2), AA6063; (c) β(1), AA6005; and (d) β(2), AA6005

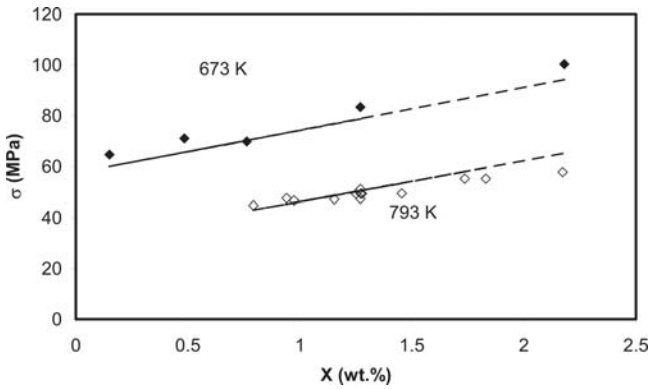

Fig. 6 Flow stress at $\varepsilon = 1$ for the two testing temperatures; data points involve both alloys and conditions WQ, β(1), and β(2) (lines, model)

during hot deformation. This assumption is justified for the PSC measurements due to the short duration (~0.012 s) of the deformation, which does not permit significant Mg_2Si dissolution. This assumption was also justified for the extrusion pressure in isothermal laboratory-scale experiments (Ref 11, 12), because thermal equilibrium was maintained during extrusion. However, in other work (Ref 15), the thermomechanical model was applied to non-isothermal industrial extrusion. In this evaluation, the thermal effects occurring during extrusion were accounted for. In the evaluation, it was found that dynamically enhanced dissolution of Mg-Si precipitates took place due to the strong deformation rate and longer times involved. This means that extrusion pressure in industrial extrusion cannot be predicted in this model as long as a static diffusion coefficient is used.

5. Conclusions

In this work, two AA6*xxx* alloys were subjected to different thermal pretreatments and were PSC tested. A previously developed constitutive model was applied to quantify the flow stresses. The following observations were made after homogenizing and quenching:

- At a testing temperature of 793 K, flow stress is highest for the nontreated condition (no precipitation), becomes lower after pre-aging leading to refined precipitates, and is lowest after pre-aging, leading to coarse precipitates. This is attributed to a decreasing solute hardening after heating up to the test temperature.
- At a testing temperature of 673 K, flow stress is highest for the nontreated condition (no precipitation), becomes lower

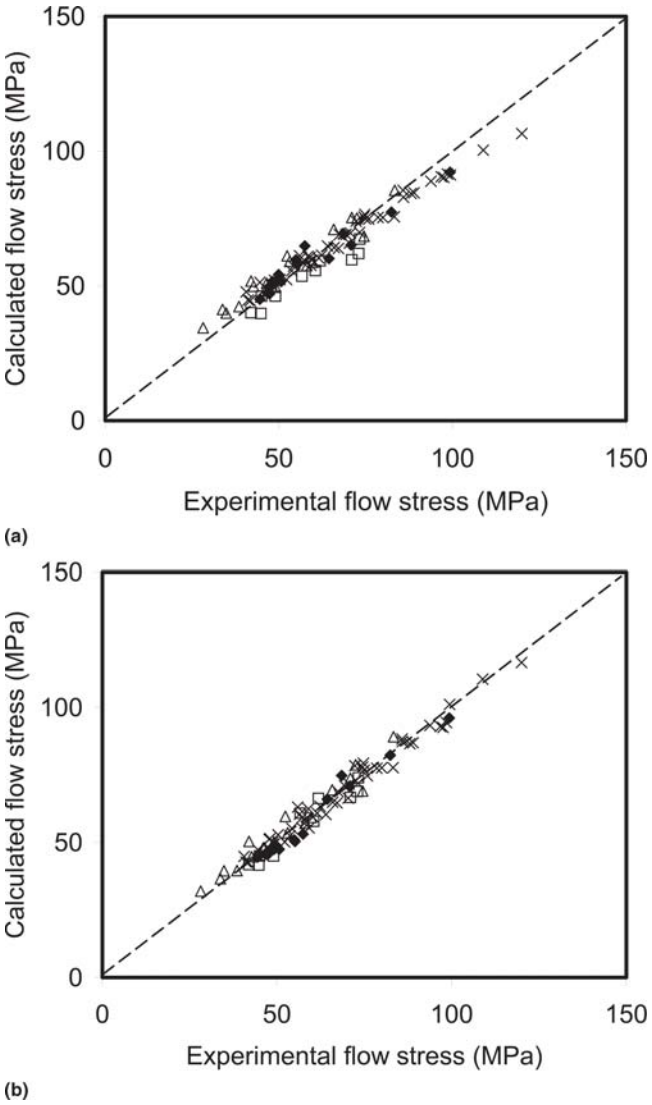

Fig. 7 Calculated flow stress against experimentally determined flow stress for several AA6*xxx* alloys and various conditions: (a) calculation according to Eq 1; (b) calculation according to Eq 1 and 2; (♦) this work; (□) Ref 6; (△) Ref 11; (×) Ref 13.

after pre-aging leading to coarse precipitates, and is lowest after pre-aging, leading to refined precipitates. Because the effect of dissolution during heating up to 673 K is less than that during heat up to 793 K, the flow stresses do not follow the same trend with pre-aging as with the 793 K testing temperature.

- A previously developed constitutive model for quantification in combination with a particle dissolution model gives a fair quantitative prediction of the present data. Furthermore, the present dataset was combined with data reported earlier. This combined set of data encompasses a wide range of alloy compositions and thermal histories.
- The model also gives a fair prediction of the flow stress for this combined set.
- An even better agreement is obtained by assuming that the parameter K_2 in the model, which describes the solution hardening behavior, is temperature dependent rather than constant.

Acknowledgments

This research was supported by the Technology Foundation (STW). The authors particularly thank Mr. N. Geerlofs and Mr. E.R. Peekstok for their technical support given with the experimental work. The authors acknowledge Prof. Dr. E. Nes of the Norwegian University of Science and Technology, Trøndheim, for suggesting the possibility of a temperature dependence of the parameter K_2 in the constitutive model.

References

1. O. Reiso, J. Strid, and N. Ryum, Melting of Secondary-Phase Particles in Al-Mg-Si Alloys, *4th Int. Conf. on Aluminum Alloys, Their Physical and Mechanical Properties,* Sept. 11-16, 1994 (Atlanta, GA), Georgia Institute of Technology, School of Materials Science and Engineering, 1994, Vol I, p 590-597
2. J. Kaneko, M.M. Sultan, and R. Horiuchi, Homogenization Heat Treatment and Hot Workability of the Ingots of Al-Mg-Si Alloys, *Z. Metallkde.,* 1976, **67,** p 8-15
3. D.H. Bratland, Ø. Grong, H. Shercliff, O.R. Myhr, and S. Tjøtta, Process Model Based Optimisation of Cooling Schedules for AA6082 Extrusions, *4th Int. Conf. on Aluminum Alloys, Their Physical and Mechanical Properties,* Sept. 11-16, 1994 (Atlanta, GA), 1994, Vol I, p 418-425
4. S. Zajac, B. Bengtsson, A. Johansson, and L.-O. Gullman, Optimization of Mg_2Si Phase for Extrudability of AA6063 and AA6005 Alloys, *Mater. Sci. Forum,* 1996, **217-222,** p 397
5. A.J. Bryant, E. Rise, D.J. Field, and E.P. Butler, Al-Mg-Si Extrusion Alloy and Method, Alcan Int., European Patent 0 222 479, granted 1989
6. J. van de Langkruis, W.H. Kool, C.M. Sellars, M.R. van der Winden, and S. van der Zwaag, The Effect of Beta, Beta′ and Beta″- Precipitates in a Homogenised AA6063 Alloy on the Hot Deformability and the Peak Hardness, *Mater. Sci. Eng. A,* 2001, **299,** p 105-115
7. F.J. Vermolen, "Mathematical Models for Particle Dissolution in Extrudable Aluminium Alloys," Ph.D. Thesis, Delft University of Technology, Delft University Press, Delft, The Netherlands, 1998
8. F.J. Vermolen, K. Vuik, and S. van der Zwaag, A Mathematical Model for the Dissolution Kinetics of Mg_2Si-Phases in Al-Mg-Si Alloys During Homogenisation Under Industrial Conditions, *Mater. Sci. Eng. A,* 1998, **254,** p 13-32
9. S.P. Chen, M.S. Vossenberg, F.J. Vermolen, J. van de Langkruis, and S. van der Zwaag, Dissolution of Beta Particles in an Al-Mg-Si Alloy During DSC Runs, *Mater. Sci. Eng. A,* 1999, **272,** p 250-256
10. J. van de Langkruis, N.C.W. Kuijpers, W.H. Kool, F.J. Vermolen, and S. van der Zwaag, Modeling Mg_2Si Dissolution in an AA6063 Alloy During Preheating to the Extrusion Temperature, *Proc. 7th Int. Aluminium Technology Seminar,* 2000 (Chicago, IL), Aluminum Association, Washington, and Aluminum Extruders Council, Wauconda, IL, 2000
11. J. van de Langkruis, R. Bergwerf, S. van der Zwaag, and W.H. Kool, Linking Plane Strain Compression Tests on AA6063 to Laboratory Scale Extrusion via Constitutive Equations, *Mater. Sci. Forum,* 2000, **331-337,** p 565-570
12. J. van de Langkruis, J. Lof, W. H. Kool, S. van der Zwaag, H. Huétink, Comparison of Experimental AA6063 Extrusion Trials to 3D Numerical Simulations, Using a General Solute-Dependent Constitutive Model, *J. Comp. Mater. Sci.,* 2000, p 381-392
13. J. van de Langkruis, W.H. Kool, and S. van der Zwaag, Assessment of Constitutive Equations in Modelling the Hot Deformability of Some Overaged Al-Mg-Si Alloys With Varying Solute Contents, *Mater. Sci. Eng. A,* 1999, **266,** p 135-145
14. J.J. Jonas, C.M. Sellars, and W.J.McG. Tegart, Strength and Structure Under Hot-Working Conditions, *Met. Rev.,* 1969, **14,** p 1-24
15. J. van de Langkruis, W.H. Kool, and S. van der Zwaag, Evaluation of the Applicability of a Thermomechanical Model to Industrial Extrusion Experiments of AA6063, *Proc. 8th Int. Aluminum Extrusion Technology Seminar ET 2004,* May 18-21, 2004 (Orlando, FL), ET Foundation, Wauconda, IL, 2004, Vol. 1, p 253-258
16. J. van de Langkruis, M.S. Vossenberg, W.H. Kool, and S. van der Zwaag, A Study on the b′ and b′′ Formation Kinetics in AA6063 Using Differential Scanning Calorimetry, *J. Mater. Eng. Perform.,* 2003, **12**(4), p 408-413

17. N.J. Silk and M.R. van der Winden, Interpretation of Hot Plane Strain Compression Testing of Aluminium Specimens, *Mater. Sci. Technol.,* 1999, **15,** p 295-300
18. F.J. Humphreys and M. Hatherly, *Recrystallization and Related Annealing Phenomena,* Pergamon, 1996
19. S.B. Davenport, N.J. Silk, C.N. Sparks, and C.M. Sellars, Development of Constitutive Equations for Modelling of Hot Rolling, *Mater. Sci. Technol.,* 2000, **16**(5), p 539-546
20. R.H. Davies, A.T. Dinsdale, J.A. Gisby, S.M. Hodson, and R.G.J. Ball, Thermodynamic Modelling Using MTDATA: A Description Showing Applications Involving Oxides, Alloys and Aqueous Solutions, *Applications of Thermodynamics in the Synthesis and Processing of Materials,* Oct. 2-6, 1994 (Rosemont, IL), 1995, p 371-384
21. M. Takeda, F. Ohkubo, T. Shirai, and K. Fukui, Precipitation Behavior of Al-Mg-Si Ternary Alloys, *Mater. Sci. Forum,* 1996, **217-222,** p 815-820
22. A.K. Gupta and D.J. Lloyd, The Precipitation in a Super Purity Al-Mg-Si Alloy, *Proc. 3rd Int. Conf. on Aluminium Alloys, Their Physical and Mechanical Properties,* June 22-26, 1992 (Trøndheim, Norway), 1992, p 21-25
23. S.P. Chen, K.M. Mussert, and S. van der Zwaag, Precipitation Kinetics in Al6061 and in an Al6061-Alumina Particle Composite, *J. Mater. Sci.,* 1998, **33,** p 4477-4483